Vol. 1 No. 2 ACTA METEOROLOGICA SINICA December 1987

A NUMERICAL SIMULATION OF THE GEOSTROPHIC ADJUSTMENT PROCESS

Chen Qiushi (陈秋士), *Lu Xianchi* (卢咸池) and *Wang Heng* (王 衡)

Department of Geophysics, Peking University, Beijing

Received November 21, 1986

ABSTRACT

In this paper, a numerical simulation of the geostrophic adjustment process with C-grid network is illustrated. A difference scheme which has the energy and potential vorticity conserving relation consistent with the differential equations is given, and the effect of some time difference schemes on dispersion of the gravity-inertia wave is discussed. An improved forward-backward time integration scheme is proposed for keeping the computational stability. The effect of various boundary conditions for a finite region model on the gravity-inertia wave is shown by some calculated results.

I. INTRODUCTION

An important problem of numerical calculation with splitting method for the atmospheric motion (Chen, 1963, 1980; Marchuk, 1968; Gadd, 1978) is how to evaluate advection and adjustment processes properly and connect them with each other. The geostrophic adjustment process has been indicated to be fundamentally a linear one, and its analytic solution has been discussed (e. g., by Kibel, 1955; Monin, 1958; Zeng, 1963; Chen and Li, 1964; etc.). In order to examine the accuracy of the difference method, it is necessary to compare the difference solution with differential one. In this paper, an attempt is to discuss the adjustment process in some details by use of difference method in order to obtain a space-time difference scheme which can correctly describe the geostrophic adjustment process.

Winninghoff (1968) found that the results of the geostrophic adjustment process simulation with difference scheme strongly depend on the distribution of variables on the grid points, and Arakawa and Lamb (1977) indicated that dispersion process of gravity wave can be better simulated with so-called "C-grid" network. Therefore the C-grid is used in the space difference scheme in this paper. As different time difference schemes can also affect the calculation results of the adjustment process, several time difference schemes are examined. Consequently, an improved forward-backward time integration scheme is proposed to remove the computational instability which appears during the calculation with unimproved one. The simulation results of the adjustment process with Euler-backward and forward-backward schemes are compared, and the effect of different lateral boundary conditions on the adjustment process simulation in a finite region is also discussed.

II. SIMPLIFIED EQUATIONS OF GEOSTROPHIC ADJUSTMENT PROCESS AND THEIR INTEGRATION CONSTRAINTS

According to the explicit splitting method of shallow-water model discussed by Chen and Lu (1983), adjustment process equations can be simplified as

$$\begin{cases} \dfrac{\partial \boldsymbol{V}}{\partial t}+f_0\boldsymbol{k}\times\boldsymbol{V}+g\nabla z=0, & (1)\\[2ex] \dfrac{\partial z}{\partial t}+H_0\nabla\cdot\boldsymbol{V}=0, & (2)\end{cases}$$

where f_0 is the mean Coriolis parameter and H_0 denotes the mean depth of the fluid.

The dot product of Eq. (1) with $H_0\boldsymbol{V}$ and multiplication of Eq. (2) with gz yield

$$\frac{\partial}{\partial t}\left(H_0K+g\frac{z^2}{2}\right)+\nabla\cdot gH_0z\boldsymbol{V}=0. \tag{3}$$

The integration of Eq. (3) in a closed region S gives

$$\frac{\partial}{\partial t}\iint_S\left(H_0K+g\frac{z^2}{2}\right)ds=0, \tag{4}$$

which means that the sum of potential and kinetic energy is conservative in a closed region during adjustment process.

Eq. (1) can be rewritten in the form of vorticity equation as

$$\frac{\partial\zeta}{\partial t}+f_0\nabla\cdot\boldsymbol{V}=0. \tag{5}$$

Substituting Eq. (2) into Eq. (5) yields

$$\frac{\partial}{\partial t}\left(\zeta-\frac{f_0}{H_0}z\right)=0, \tag{6}$$

where $\zeta-\dfrac{f_0}{H_0}z$ denotes potential vorticity. From Eq. (6) it is clear that

$$\zeta-\frac{f_0}{H_0}z=\zeta^*-\frac{f_0}{H_0}z^*=\Omega^*(x,y), \tag{7}$$

where ζ^* and z^* are the vorticity and the height of free surface at the beginning of the adjustment process, respectively, so it means that potential vorticity is time-invariable in the adjustment process.

III. THE SPACE DIFFERENCE SCHEME OF THE ADJUSTMENT PROCESS AND ITS CONSERVATION RELATION

By use of C-grid network shown in Fig. 1, Eqs. (1) and (2) can be written in Cartesian coordinates as

$$\begin{cases} \dfrac{\partial}{\partial t} u_{i,j+1/2} - f_0 \hat{v}_{i,j+1/2} + \dfrac{g}{d}(z_{i+1/2,j+1/2} - z_{i-1/2,j+1/2}) = 0, & (8) \\ \dfrac{\partial}{\partial t} v_{i+1/2,j} + f_0 \hat{u}_{i+1/2,j} + \dfrac{g}{d}(z_{i+1/2,j+1/2} - z_{i+1/2,j-1/2}) = 0, & (9) \\ \dfrac{\partial}{\partial t} z_{i+1/2,j+1/2} + \dfrac{H_0}{d}(u_{i+1,j+1/2} - u_{i,j+1/2} + v_{i+1/2,j+1} - v_{i+1/2,j}) = 0. & (10) \end{cases}$$

Here the time derivative remains in its differential form and its difference scheme will be discussed in the next section.

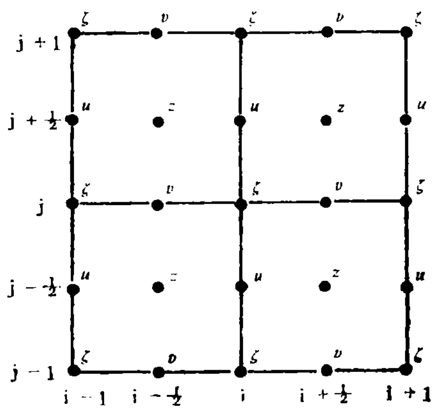

Fig. 1. Distribution of variables on the C-grid.

Let

$$\zeta_{i,j} = \frac{1}{d}(u_{i,j-1/2} - u_{i,j+1/2} + v_{i+1/2,j} - v_{i-1/2,j}) . \tag{11}$$

After differentiating (11) with respect to t and substituting Eqs. (8) and (9) into it, a vorticity equation can be obtained as

$$\frac{\partial}{\partial t}\zeta_{i,j} + \frac{f_0}{d}(\hat{v}_{i,j+1/2} - \hat{v}_{i,j-1/2} + \hat{u}_{i+1/2,j} - \hat{u}_{i-1/2,j}) = 0, \tag{12}$$

where

$$(\bar{a}^x)_{i,j} \equiv \frac{1}{2}(a_{i+1/2,j} + a_{i-1/2,j}), \tag{13}$$

$$(\bar{a}^{xy})_{i,j} \equiv \overline{(\bar{a}^x)}^y_{i,j}, \tag{14}$$

and

$$\hat{u}_{i+1/2,j} = (\bar{u}^{xy})_{i+1/2,j}, \tag{15}$$

$$\hat{v}_{i,j+1/2} = (\bar{v}^{xy})_{i,j+1/2}. \tag{16}$$

Let

$$z^{(\zeta)}_{i,j} = (\bar{z}^{xy})_{i,j}. \tag{17}$$

Derivating (17) with respect to t and substituting into (10) lead to

$$\frac{\partial}{\partial t} z_{i,j}^{(\zeta)} + \frac{H_0}{d}(\hat{v}_{i,j+1/2} - \hat{v}_{i,j-1/2} + \hat{u}_{i+1/2,j} - \hat{u}_{i-1/2,j}) = 0. \tag{18}$$

Substituting (18) into (12) yields a potential vorticity conservation relation as

$$\frac{\partial}{\partial t}\zeta_{i,j} - \frac{f_0}{H_0}\frac{\partial}{\partial t} z_{i,j}^{(\zeta)} = 0. \tag{19}$$

By integrating with respect to t, (19) can be written as

$$\zeta_{i,j} - \frac{f_0}{H_0} z_{i,j}^{(\zeta)} = \zeta_{i,j}^* - \frac{f_0}{H_0} z_{i,j}^{(\zeta)*}. \tag{20}$$

Now write the kinetic energy at z-points, and define that

$$K_{i+1/2,j+1/2} = \frac{1}{4}(u_{i+1,j+1/2}^2 + u_{i,j+1/2}^2 + v_{i+1/2,j+1}^2 + v_{i+1/2,j}^2). \tag{21}$$

Multiplying (21) by H_0, differentiating it with respect to t and substituting (8) and (9) into it yield

$$\begin{aligned}\frac{\partial}{\partial t}(H_0 K)_{i+1/2,j+1/2} = \frac{H_0}{2}\Big\{ & u_{i+1,j+1/2}\Big[f_0 \hat{v}_{i+1,j+1/2} - \frac{g}{d}(z_{i+3/2,j+1/2} - z_{i+1/2,j+1/2})\Big] \\ & + u_{i,j+1/2}\Big[f_0 \hat{v}_{i,j+1/2} - \frac{g}{d}(z_{i+1/2,j+1/2} - z_{i-1/2,j+1/2})\Big] \\ & - v_{i+1/2,j+1}\Big[f_0 \hat{u}_{i+1/2,j+1} + \frac{g}{d}(z_{i+1,j+3/2} - z_{i+1/2,j+1/2})\Big] \\ & - v_{i+1/2,j}\Big[f_0 \hat{u}_{i+1/2,j} + \frac{g}{d}(z_{i+1/2,j+1/2} - z_{i+1/2,j-1/2})\Big]\Big\}.\end{aligned} \tag{22}$$

Multiplying (10) by $g z_{i+1/2,j+1/2}$ yields a potential energy equation as

$$\frac{\partial}{\partial t}\frac{1}{2} g z_{i+1/2,j+1/2}^2 + \frac{gH_0}{d}(u_{i+1,j+1/2} - u_{i,j+1/2} + v_{i+1/2,j+1} - v_{i+1/2,j}) z_{i+1/2,j+1/2} = 0. \tag{23}$$

Adding (22) to (23) and summing up at z-points over entire region, and noticing the fact that for variables defined at the interior points on stagged grid, there is a relation as

$$\sum_{a-point} a_{i,j}(\bar{b}^{xy})_{i,j} = \sum_{b-point} b_{i+1/2,j+1/2}(\bar{a}^{xy})_{i+1/2,j+1/2}, \tag{24}$$

$$\sum_{a-point} a_{i,j}(c_{i+1/2,j} - c_{i-1/2,j}) = -\sum_{c-point} c_{i+1/2,j}(a_{i+1,j} - a_{i,j}), \tag{25}$$

and there is a similar relation with regard to the j index. Then for the adjustment process in a closed region, it follows that

$$\frac{\partial}{\partial t}\sum_{z-point}\Big(H_0 K + \frac{1}{2} g z^2\Big) = 0. \tag{26}$$

It is clear from (26) and (20) that the difference equations on C-grid satisfy the constraints (4) and (7) determined by differential equations.

IV. TIME INTEGRATION SCHEMES OF GRAVITY-INERTIA WAVES AND SOME DISCUSSIONS

Winninghoff (1968) primarily compared the dispersion relations of differential equations with time-differential and space-difference equations in different space grid networks. However, time derivation must be changed into a difference scheme in actual calculations with result that dispersion relation is also changed. So it is necessary to analyse calculation results of different-time difference schemes.

First we discuss the one-dimensional case. Eqs. (8)—(10) can be rewritten as

$$\begin{cases} \frac{\partial}{\partial t}u_j - f_0\bar{v}_j^* + \frac{g}{d}(z_{j+1/2}-z_{j-1/2})=0, & (27)\\ \frac{\partial}{\partial t}v_{j+1/2} + f_0\bar{u}_{j+1/2}^x=0, & (28)\\ \frac{\partial}{\partial t}z_{i+1/2} + \frac{H_0}{d}(u_{j+1}-u_j)=0, & (29)\end{cases}$$

where $x_j=jd$ (j=1, 2, ⋯). Let w denote the variables u, v and z, then Eqs. (27)—(29) can be rewritten in a general form as

$$\frac{\partial w}{\partial t}=f(w,t). \tag{30}$$

For Euler-backward (Matsuno) scheme, according to Eq. (30) it is seen that

$$\begin{cases} w^{n+1*}=w^n+\Delta t\cdot f^n,\\ w^{n+1}=w^n+\Delta t\cdot f^{n+1*}. \end{cases} \tag{31}$$

Let

$$w^{n+1}=rw^n, \tag{32}$$

and

$$\begin{pmatrix} u_j^n\\ v_j^n\\ z_j^n\end{pmatrix}=\begin{pmatrix}\tilde{u}\\ \tilde{v}\\ \tilde{z}\end{pmatrix}R^n e^{i(kjd-\nu n\Delta t)}, \tag{33}$$

then

$$r=Re^{-i\nu\Delta t}. \tag{34}$$

Let $w^{n+1*}=r^*w^n$, substituting (33) into (27)—(29) and using (31) to eliminate r^*, then

$$r=1\pm i\Omega\Delta t-\Omega^2\Delta t^2, \tag{35}$$

where

$$\Omega^2=f_0^2\cos^2\left(\frac{kd}{2}\right)+4\frac{gH_0}{d^2}\sin^2\left(\frac{kd}{2}\right). \tag{36}$$

Obviously,

$$|R|=\sqrt{1-\Omega^2\Delta t^2+\Omega^4\Delta t^4}, \tag{37}$$

$$|\nu|=\frac{1}{\Delta t}\tan^{-1}\frac{\Omega\Delta t}{1-\Omega^2\Delta t^2}. \tag{38}$$

It can be seen from (37) that $|R|\leqslant 1$ for $\Omega\Delta t<1$, in this case Matsuno scheme is stable. The relation diagram can be drawn according to (38) in order to illustrate the dispersion relation, which is shown in Fig. 2 for the differential, differential-difference equations and Matsuno scheme with $L_0/d=5$ $(L_0^2=gH_0/f_0^2)$. It can be seen from Fig. 2 that the dispersion relation of Matsuno scheme is similar to that of differential and differential-difference equations, and the smaller Δt is, the more similar to each other they become. Thus Matsuno scheme can describe the geostrophic adjustment process well.

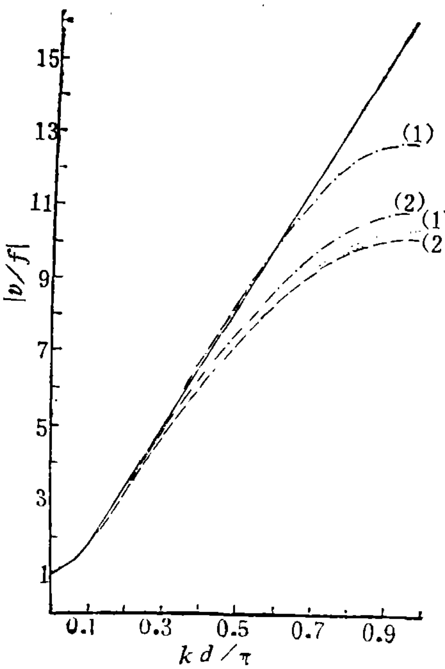

Fig. 2. Dispersion relations for different cases. Solid line: differential equations; Dashed line: differential-difference equations; Dot-dashed line: Euler-backward scheme; Dotted line: forward-backward scheme. (1) $f\Delta t=0.06$, and (2) $f\Delta t=0.03$.

However, Matsuno scheme causes wave damping when $|R|<1$, particularly for high frequency waves. According to Eqs. (1) and (2), the gravity-inertia wave is neutral, so it is dispersive but not damping. Thus Matsuno scheme would cause an artificial damping process of gravity-inertia waves which are closely related to precipitation. In addition, the scheme is only first-order of accuracy of Δt, and more computer time are required due to two-step calculation for one time step, therefore it is necessary to design a more accurate and effective scheme.

Gadd (1978) proposed a split integration scheme in which the Lax-Wendroff scheme is used to calculate the advection process and the forward-backward scheme to the adjustment process. He found that the calculation with the schemes on the C-grid network is often unstable, and Chen and Lu (1983) also obtained a similar result. Now we analyse causes for instability and then try to improve it.

For one-dimensional case, the forward-backward scheme can be written as

$$\begin{cases} u_j^{n+1}=u_j^n-\Delta t(g\delta_x z-f_0\bar{v}^x)_j^n, \\ v_{j+1/2}^{n+1}=v_{j+1/2}^n-\Delta t f_0(\bar{u}^x)_{j+1/2}^n, \\ z_{j+1/2}^{n+1}=z_{j+1/2}^n-H_0\Delta t(\delta_x u)_{j+1/2}^{n+1}, \end{cases} \tag{39}$$

where $(\delta_x\alpha)_j=(\alpha_{j+1/2}-\alpha_{j-1/2})/d$. Substituting (30) into (39) and using (32) and (34), we have

$$|R|=\sqrt{1+f_0^2\cos^2\left(\frac{kd}{2}\right)\Delta t^2}\ , \tag{40}$$

$$|\nu|=\frac{2}{\Delta t}\sin^{-1}\left(\frac{1}{2}\Omega\Delta t\right). \tag{41}$$

The dispersion relation of the forward-backward scheme has been also drawn in Fig. 2, in which we can see that the dispersion relation is well closed to that of differential-difference scheme, thus it can describe the adjustment process quite well. Only when $kd/\pi>0.5$, i. e., the wavelength is less than 4d, its dispersion relation, like that of differential-difference equations, is quite different from that of differential equations. But it is known from (40) that $|R|$ is always larger than 1 no matter how small Δt is. In other words, it is absolutely unstable even if its instability is very weak when Δt is quite small.

To avoid the increasing amplitude of difference solution with time, the forward-backward scheme can be improved by

$$\begin{cases} u_j^{n+1}=u_j^n-\Delta t(g\delta_x z-f_0\bar{v}^x)_j^n, \\ v_{j+1/2}^{n+1}=v_{j+1/2}^n-\Delta t f_0(\bar{u}^x)_{j+1/2}^{n+1}, \\ z_{j+1/2}^{n+1}=z_{j+1/2}^n-H_0\Delta t(\delta_x u)_{j+1/2}^{n+1}. \end{cases} \tag{42}$$

In the manner similar to the above derivation, when $\Omega\Delta t\leqslant 2$, it follows that

$$|R|=1, \tag{43}$$

$$|\nu|=\frac{2}{\Delta t}\sin^{-1}\left(\frac{1}{2}\Omega\Delta t\right). \tag{44}$$

Thus the improved forward-backward scheme is neutrally stable and its dispersion relation remains unchanged.

In the two-dimensional case the improved forward-backward scheme has the form

$$\begin{cases} u_{i,j+1/2}^{n+1}=u_{i,j+1/2}^n-\Delta t(g\delta_x z-f_0 v)_{i,j+1/2}^n, \\ v_{i+1/2,j}^{n+1}=v_{i+1/2,j}^n-\Delta t(g\delta_y z^n+f_0\hat{u}^{n+1})_{i+1/2,j}, \\ z_{i+1/2,j+1/2}^{n+1}=z_{i+1/2,j+1/2}^n-H_0\Delta t(\delta_x u+\delta_y v)_{i+1/2,j+1/2}^{n+1}. \end{cases} \tag{45}$$

The conclusion derived from (45) is the same as that in the one-dimensional case. When the scheme is used in time integration, both computer time and internal storage required can be saved.

V. A COMPUTATIONAL EXAMPLE OF THE BAROTROPIC ADJUSTMENT PROCESS

The character of numerical simulation for the adjustment process can be shown by a simple example. In a manner similar to that of Obukhov (1949), suppose that the initial flow field is a non-divergent circular vortex with a horizontally uniform free surface as

$$\begin{cases} \psi_0(x,y)=A\left[2+\left(\frac{R}{L_0}\right)^2-\left(\frac{r}{R}\right)^2\right]e^{-r^2/2R^2}, \\ z_0(x,y)=H_0, \end{cases} \tag{46}$$

where $r=\sqrt{(x-x_0)^2+(y-y_0)^2}$, (x_0, y_0) is the coordinates of the center of the disturbance, and $L_0=\sqrt{gH_0}/f_0$ the Rossby deformation radius. The corresponding initial wind and vorticity fields are

$$\begin{cases} u_0 = -\dfrac{\partial \psi_0}{\partial y} = \dfrac{A}{R^2}(y-y_0)\left[4+\left(\dfrac{R}{L_0}\right)^2-\left(\dfrac{r}{R}\right)^2\right]e^{-r^2/2R^2}, \\ v_0 = \dfrac{\partial \psi_0}{\partial x} = -\dfrac{A}{R^2}(x-x_0)\left[4+\left(\dfrac{R}{L_0}\right)^2-\left(\dfrac{r}{R}\right)^2\right]e^{-r^2/2R^2}, \end{cases} \tag{47}$$

and

$$\zeta_0 = \nabla^2\psi_0 = -\frac{A}{R^2}\left[8+2\left(\frac{R}{L_0}\right)^2-8\left(\frac{r}{R}\right)^2-\left(\frac{r}{L_0}\right)^2+\left(\frac{r}{R}\right)^4\right]e^{-r^2/2R^2}. \tag{48}$$

According to Obukhov (1949), the final states of the flow, free surface height and wind fields are

$$\begin{cases} \psi_\infty = A\left[2-\left(\dfrac{r}{R}\right)^2\right]e^{-r^2/2R^2}, \\ z_\infty = H_0 + \dfrac{Af_0}{g}\left[2-\left(\dfrac{r}{R}\right)^2\right]e^{-r^2/2R^2}, \end{cases} \tag{49}$$

and

$$\begin{cases} u_\infty = \dfrac{A}{R^2}(y-y_0)\left[4-\left(\dfrac{r}{R}\right)^2\right]e^{-r^2/2R^2}, \\ v_\infty = -\dfrac{A}{R^2}(x-x_0)\left[4-\left(\dfrac{r}{R}\right)^2\right]e^{-r^2/2R^2}. \end{cases} \tag{50}$$

Ageostrophic vorticity is now defined as

$$\zeta' = \nabla^2\psi - \frac{g}{f_0}\Delta^2 z. \tag{51}$$

Then on C-grid its difference form becomes

$$\zeta'_{i+1/2,j+1/2} = \zeta^{(z)}_{i+1/2,j+1/2} - \frac{g}{f_0}\,\frac{1}{d^2}(\nabla^2 z)_{i+1/2,j+1/2}, \tag{52}$$

where

$$\zeta^{(z)}_{i+1/2,j+1/2} = (\bar{\zeta}^{xy})_{i+1/2,j+1/2}, \tag{53}$$

$$(\nabla^2 z)_{i+1/2,j+1/2} = z_{i+3/2,j+1/2} + z_{i-1/2,j+1/2} + z_{i+1/2,j+3/2} + z_{i+1/2,j-1/2} - 4z_{i+1/2,j+1/2}. \tag{54}$$

Under the condition that $R=500$ km, $f_0=10^{-4}\mathrm{s}^{-1}$, $H_0=5500$ m, and $A=2.5\times10^6$ $\mathrm{m^2s^{-1}}$, the distributions of tangential wind speed v_0 and ageostrophic vorticity ζ'_0 along the X-axis cross the vortex center at initial time are shown in Fig. 3.

It is well known that the geostrophic equilibrium is reached in the adjustment process through divergence. In the region where ageostrophic vorticity is anticyclonic, the convergent flow develops to increase the geopotential height. The divergence field propagates to the surroundings in wave form. Supposing that time step $t=6$ min, space step $d=200$ km and there are 32×32 grids in the integration region, i. e., the length and width of the region are both 6200 km. The divergence distributions calculated with Euler-backward and forward-backward schemes are shown in Fig. 4. It can be seen that the convergence gradually strengthens nearby the center and the divergence occurs in the cyclonic ageostrophic vorticity region. The divergence variation with time calculated with forward-backward scheme is shown in Fig. 5, which illustrates that convergence is strong around the center when $t=0.5$ h and becomes divergent when $t=1$ h. It is obvious that divergence field

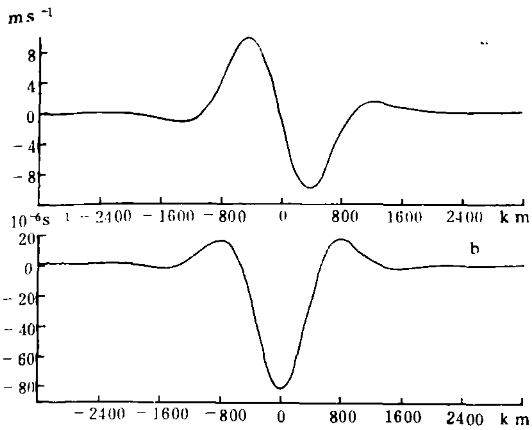

Fig. 3. Distributions along the X-axis of (a) tangential wind speed v_0, and (b) ageostrophic vorticity ζ_0'.

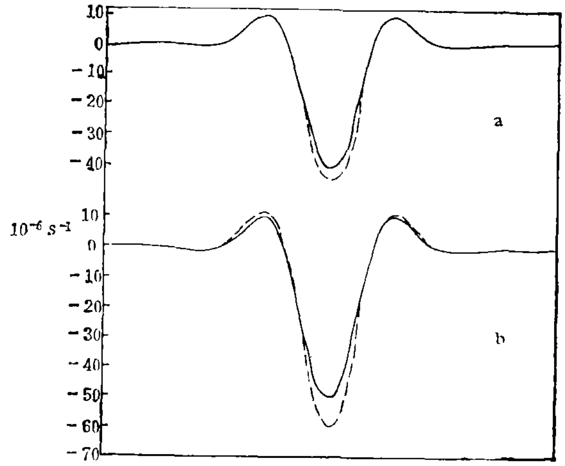

Fig. 4. Divergence distribution at (a) t=0.2 h, and (b) t=0.3 h, with solid line for Matsuno, and dashed line for forward-backward schemes.

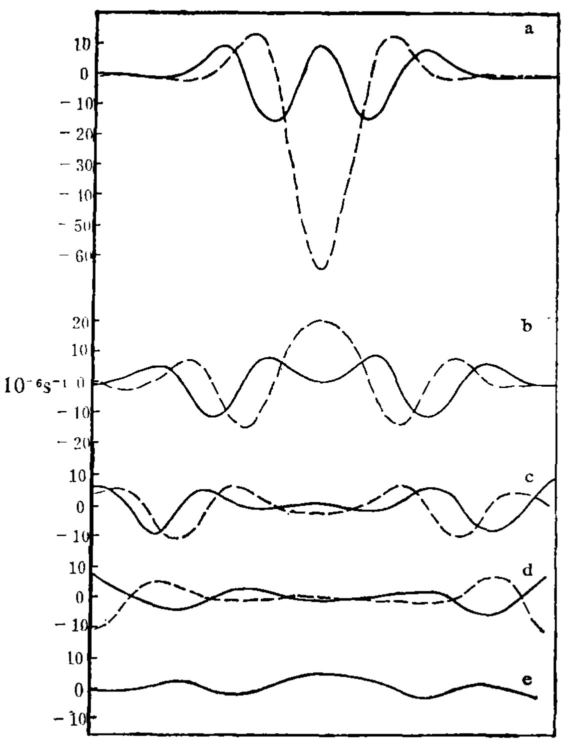

Fig. 5. Divergence distributions at different time calculated with forward-backward scheme with dashed lines for (a) 0.5, (b) 1.5, (c) 2.5, (d) 4 h, and solid line for (a) 1, (b) 2, (c) 3, (d) 5, (e) 6 h, respectively.

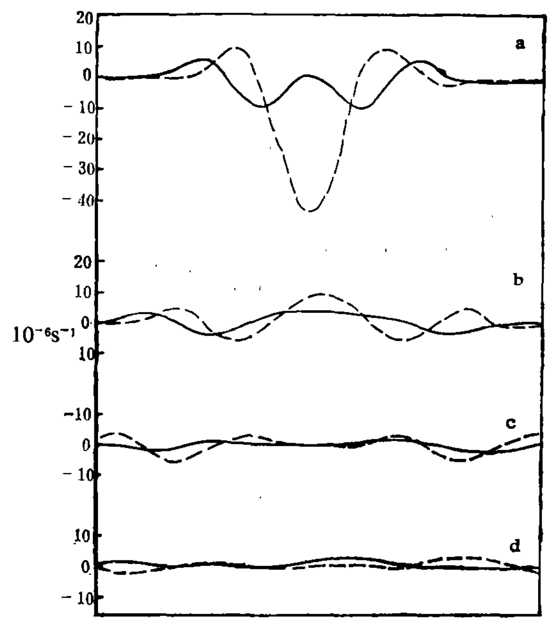

Fig. 6. As in Fig. 5., but with Matsuno scheme and dashed lines for (a) 0.5, (b) 1.5, (c) 2.5, (d) 4 h, and solid lines for (a) 1, (b) 2, (c) 3, (d) 5 h, respectively.

propagates toward the surroundings and the divergence around the center vanishes on the whole after $t=2$ h. The results calculated with Euler-backward scheme (see Fig. 6) are similar to that in Fig. 5, but the amplitude of gravity-inertia wave is much smaller.

Fig. 7 shows the temporal variation of the geopotential field along the X-axis. At the beginning, the geopotential field is uniform (not shown), then a high center is established by adjustment process. It can be seen from Fig. 7 that in the central region the geopotential is highest at $t=1$ h and then decreases, after $t=3$ h a high remains there and its strength changes very little.

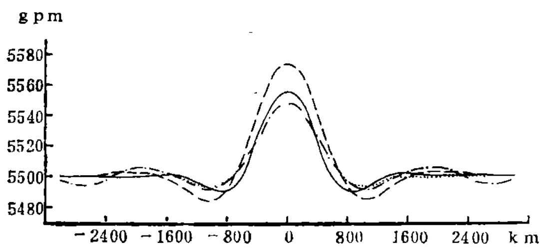

Fig. 7. Geopotential distributions in adjustment process at different time. solid line: 0.5 h. Dashed line: 1 h. Dot–dashed line: 3 h. Dotted line: 6 h.

Fig. 8 is the distributions of the tangential speed v along the X-axis at $t=1$ h calculated with Euler-backward and forward-backward schemes. Maximum wind speed slightly

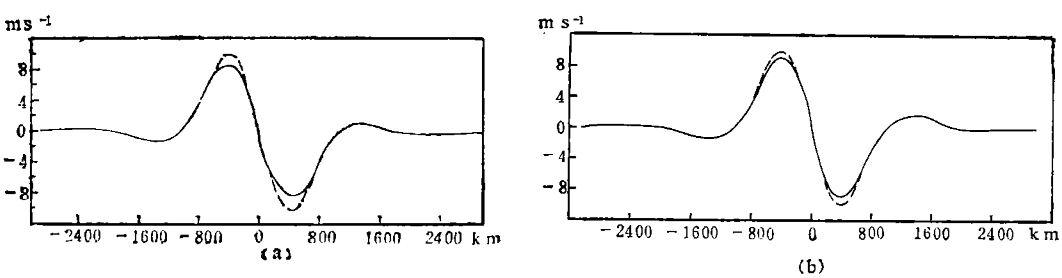

Fig. 8. Distribution of tangential wind speed v along X–axis in the adjustment process calculated with (a) Euler-backward, (b) forward–backward schemes. Dashed line: $t=0$ h, and solid line: $t=1$ h.

decreases compared with that at initial time. After then it changes very little (not shown). The wind speed calculated with the forward-backward scheme is a little larger than that with Matsuno scheme. The difference of the central wind speeds is less than 1 m/s before and after the geostrophic adjustment process.

Several investigators (Chen, 1963, 1980; Zeng, 1963) have indicated that the geopotential field is mainly adjusted to the flow field if the horizontal scale of the disturbance, L, is smaller than L_0. So is that in the example. Shown in Fig. 9 is the distribution of z_∞ and v_∞ along the X-axis at the end of the adjustment process calculated with Eqs. (49) and (50). Obviously, the solutions of difference and differential equations resemble each other

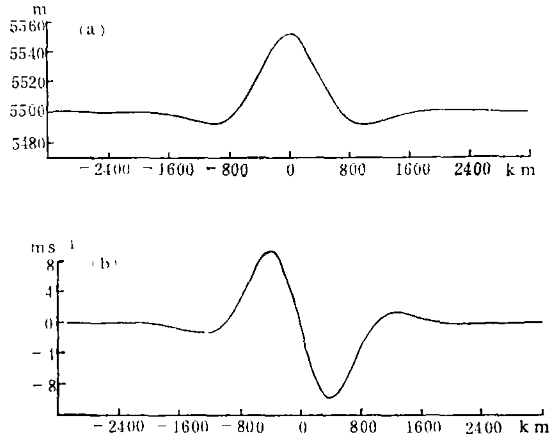

Fig. 9. Distribution of (a) free surface height z_∞, and (b) tangential wind speed v_∞ along X-axis.

very well.

The above analysis is mainly the calculated results before $t=6$ h. As the integration time extends, the effect of the boundary becomes significant and different results appear during numerical simulations according to different boundary conditions.

In the geostrophic adjustment process, the wave energy disperses to infinite distance in the form of gravity-inertia wave, so that the geostrophic equilibrium can be established. But during numerical simulations, the integration is carried out in a finite region and then boundary condition problem must be accounted for. In numerical models, the boundary condition can be determined by several ways, such as (1) fixed boundary, (2) interpolation from forecasting data of a coarse grid in a large region, (3) to be assigned by the data at interior points, and (4) so-called "sponge layer" (hereinafter referred to as conditions 1—4). These methods are very simple, but have some shortcomings. The solution nearby the outflow boundary is determined by solutions in the interior region. The boundary condition defined artificially would make the equation ill-posed, so that the difference between the data defined artificially in the boundary and determined by the interior solution may cause a strong geostrophic wind deviation nearby the boundary and then a spurious strong gravity-inertia wave which propagates back into the interior region.

To avoid the computational instability caused by the spurious gravity-inertia wave in the boundary region, smoothing is often used to damp the energy of gravity waves. However, for keeping the equations well-posed there is a more reasonable way, in which only a part of boundary values required by the linear system corresponding to the difference equations are defined and others are determined by an extrapolation method. That is so-called "open boundary". Hack and Schubert (1981) used the boundary condition with the form in cylindrical coordinates as

$$\frac{\partial V_n}{\partial t}+\frac{c_n}{\sqrt{r}}\frac{\partial rV_n}{\partial n}=0. \tag{55}$$

In our simulation several boundary conditions are examined and results with or without smoothing nearby boundaries are also compared. The sponge boundary condition to be used is

$$\phi_j^{(n)} = \phi_j^{(n-1)} + W_j \left(\frac{\partial \phi}{\partial t} \right)_j \Delta t, \tag{56}$$

with W_j being weight coefficient and it is defined that $W_j = 0$ when $j = 1, J$; $W_j = 0.4$ when $j = 2, J-1$; $W_j = 0.7$ when $j = 3, J-2$; $W_j = 0.9$ when $j = 4, J-3$; and $W_j = 1.0$ when $4 < j < J-3$. Here J is the maximum j index.

According to the open boundary condition (hereinafter referred to as condition 5), the wind speed normal to the boundary in outflow region is defined to satisfy

$$\frac{\partial V_n}{\partial t} + c_n \frac{\partial V_n}{\partial n} = 0, \tag{57}$$

and the tangential wind speed in the boundary of inflow region is defined to be invariable.

Divergence fields at $t = 12$ h calculated with different boundary conditions are shown in Fig. 10. According to the result with condition 1 (see curve a in Fig. 10), the divergence field does not tend to zero as time increasing because of strong boundary reflection; condition 2 is not adopted; the result calculated with condition 3 is similar to that with condition 1 (not shown); the result calculated with condition 4 (see curve b) shows divergence with strength slightly smaller than that shown as curve a; but if a 5-point smoothing operator in the first cycle of the interior region is added to condition 4, the divergence decreases significantly (see curve c); and the divergence calculated with condition 5 is the smallest (see curve d).

Hence it is obvious that the open boundary condition, or sponge boundary condition with a suitable smoothing is the best fit for simulating the dispersion of gravity-inertia wave properly.

VI. CONCLUSIONS

(1) A difference scheme of the equations or the adjustment process on C-grid is proposed and it is proved that the energy and potential vorticity conservation relations in space difference scheme are all the same as that in differential equations.

(2) The dispersion features of Matsuno and forward-backward time integration schemes are discussed, and an improved forward-backward scheme is proposed to make difference solution neutrally stable.

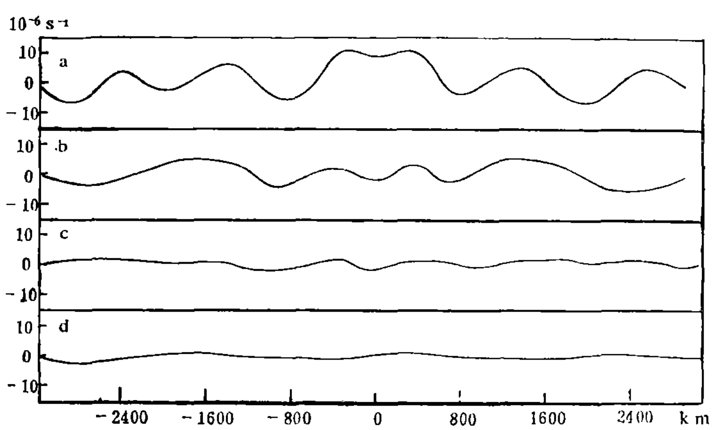

Fig. 10. Divergence distribution along X-axis at $t = 12$ h calculated with different boundary conditions.

(3) A computational example of the adjustment process shows that the simulation of the geostrophic adjustment process with both Matsuno and forward-backward time integration schemes is effective. The simulations calculated with these schemes are similar to each other, but the gravity-inertia wave amplitude calculated with forward-backward scheme is larger than that with Matsuno scheme.

(4) The effect of lateral boundary conditions on the propagation of gravity-inertia wave is studied and it is indicated that the dispersion of gravity-inertia wave can be properly simulated with the open boundary condition.

REFERENCES

Arakawa, A., and Lamb, V. R. (1977), Computational design of the basic dynamical process of the UCLA general circulation model, *Methods in Comput. Physics,* Vol. 17, Academic Press, pp. 173—265.

Chen Qiushi (1963), On the formation and destruction of the thermal wind balance in a simple baroclinic atmosphere, *Acta Met. Sinica,* **33**: 51—63, 153—162 (in Chinese).

——(1980), An explicit splitting computational method for analysing the physical processes of atmospheric motion, *Proceedings of the Second National Symposium on Numerical Weather Prediction,* Academic Press, Beijing, pp. 271—282 (in Chinese).

Chen Qiushi and Li Mingde (1964), Thermal wind adjustment in a 4-layer model, *Acta Met. Sinica,* **34**: 253—270 (in Chinese).

Chen Qiushi and Lu Xianchi (1983), An explicit splitting method of shallow-water model with terrain effect and its experiment (in Chinese, to be published).

Gadd, A. J. (1978), A split explicit integration scheme for numerical weather prediction, *Quart. J. R. Met. Soc.,* **104**: 569—582.

Hack, J. J. and Schubert W. H. (1981), Lateral boundary conditions for the tropical cyclone models, *Mon. Wea. Rew.,* **109**: 1404—1420.

Kibel, I. A. (1955), On the adjustment of atmospheric motion to geostrophic equilibrium, *Reports A.S. U.S. S.R.,* **104**: 60—63 (in Russian).

Marchuk, G. I. (1968), Short term weather prediction by splitting of the complete hydrodynamic equations, *Proc. WMO/IUGG Symp. Num. Wea. Pred.,* Tokyo, II, pp. 1—8.

Monin, A. S. (1958), On pressure change in baroclinic atmosphere, *Bulletin A.S. U.S.S.R., T. Geophys.,* **4**: 497—514 (in Russian).

Obukhov, A. M. (1949), On geostrophic wind, *Bulletin A.S. U.S.S.R., T. Geography and Geophys.,* **13**: 281—306 (in Russian).

Winninghoff, F. L. (1968), On the adjustment toward a geostrophic balance in a simple primitive equation model with application to the problems of initialization and objective analysis, Ph. D. thesis, Dept. of Meteorology, Univ. of Calif. Los Angels, 161pp.